

The radio and X-ray properties of Abell 2255

L. Feretti^{1,2}, H. Böhringer³, G. Giovannini^{1,2}, and D. Neumann³

¹ Istituto di Radioastronomia – CNR, via Gobetti 101, I-40129 Bologna, Italy.

² Dipartimento di Astronomia dell'Università, Via Zamboni 33, I-40126 Bologna, Italy.

³ Max Planck Institut für Extraterrestrische Physik, PO Box 1603, D-85740 Garching, FRG

October 15, 2018

Abstract. New radio and X-ray data are reported for the rich cluster Abell 2255. The cluster radio emission is characterized by the presence of a diffuse halo source, located at the cluster center, and a more peripheral ridge of radio emission which could be a relic. In addition, 6 tailed radio sources and a small double are found to be associated with cluster galaxies. At X-ray wavelengths, the cluster shows elongated emission in the center, indicating an ongoing cluster merger, with the axis in the east-west to southeast-northwest direction. The overall cluster temperature is found from the ROSAT observation to be $kT = 3.5(\pm 1.5)$ keV, while the temperature determined from the Einstein MPC data was reported to be 7.3 keV. We interpret this difference as due to the existence in the cluster of several coexisting temperature components.

The merger process can provide energy to maintain the radio halo, but we stress the need for tailed radio galaxies orbiting at the cluster center to provide the halo relativistic electrons.

1. Introduction

Recent observations of clusters of galaxies have revealed a new and complex scenario in the structure of the intergalactic medium. The clusters are not simple relaxed structures, but are still forming at the present epoch. Substructures, commonly observed in the X-ray distribution of a high number of rich clusters (Henry & Briel 1993, Burns et al. 1994), are evidence of hierarchic growth of clusters from the merger of poorer subclusters.

An important problem in cluster phenomenology regards cluster-wide radio halos, whose prototype is Coma C (Giovannini et al. 1993, and references therein). These are extended diffuse radio sources with typical sizes of 0.8–1.2 Mpc ($H_0=50$ km s⁻¹ Mpc⁻¹) and steep radio spectra. Their origin and properties are still poorly understood.

Send offprint requests to: L. Feretti

According to recent suggestions, the cluster merger process may play a crucial role in the formation and energetics of these sources (see Feretti & Giovannini 1996 and reference therein).

We present here radio and X-ray data of the cluster Abell 2255, known to contain a diffuse radio halo (Jaffe & Rudnick 1979, Harris et al. 1980, Burns et al. 1995) and characterized by the presence of several tailed radio galaxies. It is located at the redshift of 0.0809 (Postman et al. 1992). From the optical point of view, this cluster is classified as RS type C (Struble & Rood 1982) and shows a radial velocity dispersion of 1221 km s⁻¹, one of the largest observed for any cluster (Zabludoff et al. 1990). Analysis of the spatial and redshift distribution of cluster galaxies (Zabludoff et al. 1990) shows no evidence of optical subclumps. At X-ray wavelengths, a temperature of 7.3 keV is reported by David et al. (1993), and no cooling flow has been detected (Edge et al 1992).

In this paper, the radio and X-ray observations of A2255 are analysed to derive the connection between the X-ray and radio properties. We also discuss the physical conditions of the intergalactic medium and of the radio halo and extended radio galaxies. With the adopted value $H_0=50$ km s⁻¹ Mpc⁻¹, 1 arcsec corresponds to 2.01 kpc.

2. Radio Data



Fig. 1. Radio map at 90 cm with resolution of $89'' \times 84''$ (@6°). The σ noise level in this map is 1.3 mJy/beam. Contours are -4, 4, 7, 10, 20, 30, 50, 70, 100, 300, 500, 1000 mJy/beam. Crosses indicate the radio galaxies.

Two full synthesis observations were obtained with the Westerbork Synthesis Radio Telescope (WSRT) in January and May 1992, at 90 and 20 cm, with short spac-

ings of 36 and 72 m, and 36 and 54 m, respectively. Data were calibrated using the Dwingeloo Westerbork Astronomical Reduction Facility package (DWARF) and further reduced with the Astronomical Image Processing System (AIPS), following the standard procedure (Fourier inversion, CLEAN and RESTORE).

The angular resolutions of the final maps at 90 and 20 cm are $\sim 85''$ and $\sim 12''$, respectively. In addition to the full resolution map, a map degraded to a lower resolution was produced at 20 cm by omitting the longest baselines, in order to enhance the low brightness structure. A spectral index map was produced comparing two maps obtained with the same UV coverage. We also obtained maps of the polarized intensity in the standard way.

2.1. Diffuse halo

The radio image of the cluster center at 90 cm is presented in Fig. 1. Extended emission is detected from cluster galaxies, indicated in Fig. 1 by crosses. Moreover, the radio emission is characterized by the diffuse halo, showing one component at the cluster center (A), and a more peripheral component of very elongated shape (B). This last feature, which has been mapped for the first time by Burns et al (1995), is not obviously associated with any cluster galaxy. The component A shows here a size much larger than in the previous maps by Harris et al. (1980) and Burns et al. (1995), owing to the high sensitivity of the present map to the extended regions of low brightness and steep spectrum. The centroid of the halo region (component A) is about RA(J2000) = $17^h 12^m 45^s$, DEC(J2000) = $64^\circ 04' 30''$.



Fig. 2. Radio map at 20 cm, convolved to the resolution of $70''$ (HPBW). The σ noise level is 0.1 mJy/beam. Contours are $-0.5, 0.3, 0.5, 0.7, 1, 1.5, 2, 3, 5, 7, 10, 30, 50, 100, 150, 200$ mJy/beam. Large negative residuals are due to the lack of short spacings in the UV data.

At 20 cm, the diffuse halo is below the sensitivity of the full resolution map, but is visible in the lower resolution map (Fig. 2), where the signal to noise ratio is improved. The extended emission in this map is clumpy, and in the northwestern halo region has the shape of a ring. This structure is in good agreement with the VLA map obtained by Burns et al. (1995) at 20 cm and is also present in our 90 cm map, less clearly because of the larger beam.

The flux density, angular size, and intrinsic parameters for the diffuse source components are given in Table 1.

The integrated spectrum of the extended emission between 90 and 20 cm is $\alpha_{20}^{90} \sim 1.7$. The spectral index dis-

Table 1. Diffuse source

	Component A	Component B
S - 90 cm (mJy)	536	103
S - 20 cm (mJy)	43	12
Largest Size (kpc)	1200	965
Luminosity (W)	1.6×10^{34}	2.2×10^{33}
Volume (kpc ³)	4.7×10^8	3.7×10^7
u_{min} (erg cm ⁻³)	2.1×10^{-14}	1.9×10^{-14}
U_{min} (erg)	2.9×10^{59}	2.1×10^{58}
H_{eq} (μ G)	0.48	0.45

tribution of the halo between 90 and 20 cm is difficult to obtain, because the subtraction of extended radio galaxies present within the diffuse emission is tricky especially at 20 cm. As a general trend, we obtain a fairly constant steep spectrum in the halo region, with $\alpha > 1.5$, and no strong evidence of steepening in the outermost region. An evident steepening is instead present in the "hole" region, where we derive a spectral index > 2 . The spectrum of the northern elongated ridge (component B) is fairly constant and slightly flatter, with spectral index around 1.3-1.5.

We made polarization maps of the cluster at both frequencies. At 20 cm, polarized flux is detected from all the extended radio galaxies, but not from the diffuse emission. This implies an upper limit to the polarized brightness of the halo of 0.1 mJy/beam, and an upper limit to the polarized flux percentage of $\sim 9\%$. At 90 cm, no significant polarized flux is detected either in the halo or the extended radio galaxies. This implies an upper limit of $\sim 2\%$ for the halo polarization percentage.

2.2. Radio galaxies

In the full resolution image at 20 cm, five tailed radio sources and a small double can be identified with cluster galaxies, in accord with Harris et al. (1980). Another tailed radio source, B1713+643, is found to be coincident with a 18.2^m galaxy of unknown redshift. This source was detected also by Harris et al. (1980), but was unresolved in their observations. Owing to its morphology, we favour the hypothesis that this source also is a cluster radio galaxy.

The cluster radio galaxies showing extended structure are listed in Table 2, where the position refers to the optical galaxy. They are marked by crosses in Fig. 1, while their high resolution radio images are presented in Fig. 3.

In the sources 1711+640, 1712+640 and 1712+641 the nucleus and jets are not resolved. The tail transverse size in 1712+640 is rather constant, indicating the efficiency of confining effects. In the low resolution map, this source shows a sharp bend to the north (see Fig. 2) where it merges into the halo. A similar structure is seen in the tailed radio galaxy NGC4869, which merges into the Coma

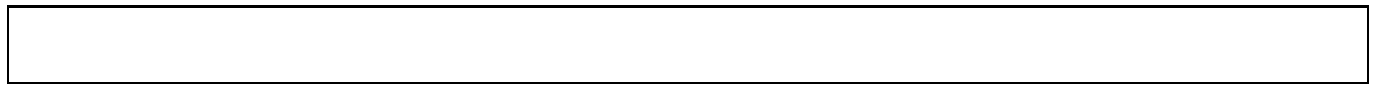


Fig. 3. Radio maps of the individual radio galaxies, at 20 cm, with the resolution of about $12.7'' \times 11.6''$ ($\sim 2^\circ$). The noise r.m.s. in the maps is 0.05 mJy/beam. Contour levels are: -0.3, 0.3, 0.7, 1.5, 3, 5, 10, 25, 50, 100 mJy/beam for 1712+640 and 1713+641; -0.15, 0.15, 0.3, 0.5, 0.7, 1, 2, 3, 5, 10, 20 for the others.

Table 2. Properties of extended radio galaxies

Radiogal.	WSRT#	RA(J2000)	DEC	S ₉₀	S ₂₀	Struct.
	14W	h m s	° ' "	mJy	mJy	
B 1711+640	113	17 12 16.2	64 02 06	1282.4*	10.7	Tail
B 1712+640	115	17 12 24.6	64 02 08		303.2	Tail
B 1712+641	118	17 13 04.8	64 06 59	202.4	64.8	Tail
B 1712+638	119	17 13 16.5	63 47 42	296.2	82.7	Tail
B 1713+641	120	17 13 29.3	64 02 49	597.3	276.65	Double
B 1713+643	123	17 14 05.6	64 16 02	28.4	7.3	Tail
B 1714+641	127	17 15 09.0	64 02 54	186.6	57.5	Tail

*This flux refers to the sum of 1711+640 and 1712+640, which are blended in the 90 cm map

cluster radio halo and is suggested to be responsible for the relativistic electron supply to the halo itself (Giovannini et al. 1993). The tail of 1712+641 is very narrow, with the transverse size unresolved by the $\sim 12''$ observing beam. The source 1712+638 resembles the prototype head-tail galaxy NGC 1265 in the Perseus cluster (O’Dea & Owen 1986), but again the transverse size of the tail is narrow, with a pinch at about $1.5'$ from the core. In 1714+641, the twin opposite jets are well visible. They end in faint hot spots, from which low brightness tails originate. This source is likely to be affected by projection effects.

Finally, we remark the peculiarity of the source 1713+641, which shows a double structure with separation of $\sim 20''$ (40 kpc). At higher resolution (Rudnick & Owen 1977), this source shows the typical Fanaroff-Riley II structure (Fanaroff & Riley 1974) with a faint core and two symmetric lobes. The double radio structure is rare in clusters (Fanti 1984); moreover, this source is very small for its power of 8×10^{24} W/Hz at 1.4 GHz (see the size-power relation of radio galaxies in clusters, Feretti & Giovannini 1993).

3. X-ray Data

3.1. Spatial analysis

A2255 was observed by us with the ROSAT High Resolution Imager (HRI) detector, in two pointings in January and June 1994, for a total of $\approx 32,500$ sec. A 14,500 sec exposure, obtained with the Position Sensitive Proportional Counter (PSPC), was taken from the ROSAT archive. The ROSAT energy band is 0.1-2.4 keV for both detectors. The HRI provides high angular resolution (nominally FWHM

$\sim 2''$), while the PSPC has an angular resolution of $\sim 25''$ (FWHM) at 1 keV, as well as energy resolution. A detailed description of the instruments can be found in Trümper (1983) and Pfeffermann et al. (1987). The data analysis has been performed with the EXSAS package (Zimmerman et al. 1994). Maps of X-ray brightness distribution were produced by binning the photon events in a two-dimensional grid and then smoothing with a gaussian filter. The PSPC image was made in the hard band, corresponding to the energy range 0.5-2.0 keV.




Fig. 4. ROSAT/PSPC image of A2255. The image is filtered with a gaussian of $50''$ (FWHM). The contour levels are 0.025, 0.04, 0.065, 0.1, 0.17, 0.25, 0.4, 0.6 count s^{-1} pixel $^{-1}$ (1 pixel = $15'' \times 15''$). The background is about 0.012 count s^{-1} pixel $^{-1}$.




Fig. 5. ROSAT/HRI contours of A2255, superimposed on the grey-scale image from the digitized Palomar Sky Survey. To enhance low brightness structure, the X-ray image is smoothed with gaussians of increasing width with decreasing count rate, from $10''$ to $50''$ (FWHM). The contour levels are 0.7, 0.8, 0.9, 1, 1.1, 1.2, 1.3, 1.4, 1.5 counts/pixel (1 pixel= $4'' \times 4''$).

Figs. 4 and 5 show PSPC and HRI images of A2255, respectively. The X-ray emission shows elliptical structure in the PSPC, confirmed by the high resolution HRI image. In the outer low surface brightness region the cluster appears to be more symmetric. The centroid of the X-ray emission is approximately RA(J2000)=17^h12^m45^s, DEC=64°03'54". The X-ray peak is shifted to the west with respect to this position.

A radial profile of the X-ray surface brightness was obtained by integrating the PSPC counts over concentric annuli of 15", centered on the approximate symmetry center. Similarly, a radial profile of the HRI X-ray emission was obtained by integrating the photon counts over concentric annuli of 8". In this averaging process any deviations from symmetry are neglected. The profiles were fit with a hydrostatic isothermal model described by the functional form (Cavaliere & Fusco-Femiano 1981, Sarazin 1986):

$$S(r) = S_0(1 + r^2/r_c^2)^{-3\beta+0.5}$$

where S_0 is the central surface brightness, r_c is the core radius, and β is the ratio of the galaxy to gas temperature. The cluster background is also fit. The parameters obtained from the fit to the PSPC profile are $r_c=4.8' \pm 0.4'$ and $\beta=0.74 \pm 0.04$, in excellent agreement with the values $r_c=4.92'$ and $\beta=0.77$ obtained by Jones & Forman (1984) with the Einstein Observatory in the 0.5-3 keV energy range. The profile is shown in Fig. 6. The fit to the HRI surface brightness profile is problematic, because the cluster extends over the whole field of view and therefore the profile does not reach the background. However, the model obtained from the PSPC fit provides a very good fit also for the HRI data. Therefore, a single β model fit can satisfactorily reproduce the X-ray brightness profile.



Fig. 6. Surface brightness profile of A2255 from the PSPC data. The full line shows the fit of the β model.

The asymmetric structure of the cluster is shown in detail if the spherically symmetric cluster component corresponding to the best-fitting azimuthally averaged β model is subtracted from the X-ray image. Apart from discrete sources, the main residuum is in the eastern sector. This decomposition is not perfectly unique, however, since the results depend on the choice of the center of symmetry. We have chosen as symmetry center the X-ray maximum located approximately in the center of the innermost elliptical contour of the PSPC image, and a bit to the east in the innermost elongated contour of the HRI image. The fact that the cluster in the PSPC image appears more elongated to the east and southeast, with respect to the X-ray peak, now gives rise to the compact structure in the

residuum shown in Fig. 7. In the innermost region, there is also a small region of excess emission lying west of the adopted center. At larger radii, one also observes very low surface brightness emission in the northwest (opposite the more prominent substructure in the southeast) in which a cluster of point sources is embedded. Even though this low surface brightness emission is probably real its significance is not high and it falls below the first contour in Fig. 7. The overall morphology of the X-ray image leads to the conclusion that this cluster is another example of merging subclusters (see also Burns et al. 1995). Compared to the case of A2256 (Briel et al. 1991) where the infalling sub-cluster could be well separated, it is more difficult here to unravel the merger structure. But the situation suggests that the major merger axis is in the east-west to southeast-northwest direction.



Fig. 7. Residual of the ROSAT/PSPC image, after subtraction of a symmetric β model. No negative contours are plotted, since they only contain noise and no significant structure.

3.2. Spectral analysis

We have analysed the X-ray spectra from the PSPC observation both in the whole cluster and in several concentric rings around the cluster center. Since the cluster is elongated in the east-west direction, which may also be the axis of the possible cluster merger, we also looked for differences in the eastern compared to the western sectors. The X-ray spectra in the studied areas are background-subtracted using regions in a ring between 25' and 33' radius.

The spectra were analysed by fitting models of the emission of hot, optically thin plasma (Raymond & Smith 1977) with the hydrogen column density, N_H , the plasma temperature, kT , the relative abundance of heavy elements, and the normalization amplitude as fit parameters. The hydrogen column density was found to be generally close to the expected galactic absorption. The heavy element abundance of the emitting material was generally fixed to 0.35 times the solar value. Tests with values in the range 0.2 - 0.5 times the solar values (the typical range observed for clusters, Ohashi 1995) showed that the variation of this parameter has little influence on the results for the other parameters.

The overall temperature found for the cluster is $kT = 3.5(\pm 1.5)$ keV. There is no significant difference in the results for the inner region inside a radius of 5' and the outer region to 10' or 20' radius. The temperature for this cluster determined from the MPC data obtained with the

EINSTEIN observatory (David et al. 1993) gave a value of $7.3^{+1.7}_{-1.1}$ keV, which is consistent with the high velocity dispersion of this cluster. There seems to be a clear discrepancy between these results, unless the cluster has several coexisting temperature components. Analysis made with data of the EINSTEIN MPC, which has a higher energy window, is more sensitive to the cut-off of the X-ray continuum spectrum towards high energy. Therefore the highest temperature component is most sensitively detected. The ROSAT energy window (0.1 - 2.4 keV) does not cover the energy range of the spectral cut-off, and the analysis of the PSPC data tends to give more weight to the low temperature components. Unfortunately, the limited energy discrimination of the ROSAT PSPC and the limited photon statistics of the present data set does not allow for a meaningful multitemperature fit, which would greatly increase the number of free fitting parameters. Therefore, we can only tentatively conclude that the discrepancy between the two instruments may imply a multiphase cluster medium, with unresolved temperature variations. This expectation would also be in line with the interpretation of the cluster as being in a state of merging.

Burns et al. (1995) found an even lower temperature of $1.9^{+2.4}_{-0.4}$ in the central $5'$ radius region, and interpreted this as a temperature drop to the center. In the light of the above results, this is not due to a spatial temperature variation and is consistent with our value within the errors.

A comparison of spectra of the two sectors in different ring areas shows that the spectra from the eastern region are significantly harder than those from the western parts. It is very difficult, however, to assign a temperature difference to this difference in hardness, because of variation also in the absorbing hydrogen column density and in the heavy element abundance.

4. Discussion

4.1. Halo origin

The diffuse halo in A2255 is comparable in size to the prototype halo source in the Coma cluster, Coma C (Giovannini et al. 1993), but is more irregular in the brightness distribution. A map of the diffuse radio emission at 90 cm, after subtraction of the imbedded extended sources, is shown superimposed on the X-ray image in Fig. 8. It is evident that the main radio halo is located at the center of the X-ray brightness distribution, as can also be deduced from the positions of the halo centroid (sect. 2.1) and the X-ray centroid (sect 3.1).

The northern ridge (component B) is at the boundary of the X-ray emission, and is not obviously related to any X-ray substructure. It is also unclear if it is related to component A. It could be located in a cluster peripheral region, at a true distance much larger than the projected distance, and could be classified as a relic source.



Fig. 8. Contours of the halo image at 90 cm, after subtraction of discrete sources, superimposed on the greyscale X-ray PSPC image. Contour levels are -4, 4, 7, 10, 15, 20, 25, 30 mJy/beam.

The properties of radio halo and relics in clusters have been recently reviewed by Feretti & Giovannini (1996). While the origin of relics is still puzzling, the existence of central halos is likely to be associated with a cluster merger process, providing the energy necessary for particle reacceleration and magnetic field amplification. The merger hypothesis alone, however, cannot explain the statistics of radio halos; radio halos are rare, while mergers in clusters seem common. In the case of Coma-C, Giovannini et al. (1993) suggested that the tailed radio galaxy NGC4869, orbiting around the cluster center, is responsible for the relativistic electron supply. The requirement of tailed radio galaxies residing at the cluster centers as the origin of relativistic particles could explain the rarity of halo type radio sources.

A2255 fits the previous picture, owing to the existence of a cluster merger and the presence of three tailed radio galaxies at the cluster center, within the halo region. The halo is not spherically symmetric, but elongated in the east-west direction, i.e., in the merger direction. This structure is therefore a strong point in favour of a connection between the merger and the radio halo. Moreover, the halo spectrum shows an evident steepening in the north-western region (see Sect. 2.1), i.e., opposite to the merger. Here, the electron reacceleration is likely to be less efficient. We note here that the double radio galaxy 1713+641 lies exactly in the merger region. An attractive possibility to explain its small size and lack of distortion is that this is a young source triggered by the merger.

The orientations of tails of the tailed radio galaxies with respect to the cluster center provide clues to the distribution of galaxy orbits within the cluster (O’Dea et al. 1987). The three tailed radio galaxies embedded within the halo radio emission, i.e., 1711+640, 1712+640, and 1712+641, actually show tails oriented at random angles with respect to the cluster center, and are therefore likely to be in random orbits at the cluster center. They could be responsible for the deposit of relativistic particles radiating in the halo, as discussed above.

4.2. Cluster Mass

Under the simple assumptions of hydrostatic equilibrium in the intracluster medium and spherical symmetry of the cluster it is possible to determine the total cluster mass from the gas density and temperature distribution. The validity of these assumptions was studied in N-body/hydrodynamic simulations of cluster formation by

Schindler (1996) and Evrard et al. (1996). These authors in particular studied how well the cluster mass determined under these assumptions is consistent with the true mass of the model cluster for cases where the cluster is approaching the equilibrium configuration. In A2255 the merging subcluster probably has already fallen far into the center of the main cluster and passed the central region of the main cluster. This interpretation is implied by the fact that the two bright galaxies are no longer coincident with a maximum of the X-ray surface brightness. Burns et al. (1995) also come to this conclusion after a comparison of the X-ray and optical appearance of the cluster with a set of possible model clusters from N-body/hydrodynamical simulations. In this configuration, the cluster mass determined under the assumption of hydrostatic equilibrium agrees within about 20% with the true cluster mass (except for the radial region around the location of the major outgoing thermalizing shock wave, Schindler 1996). Therefore we can get a good account of the total cluster mass by using the above obtained information on the density distribution and the temperature of the intracluster plasma. The errors due to deviations from symmetry and hydrostatic equilibrium are in this case very likely smaller than the uncertainties introduced due to the imprecise knowledge of the temperature profile.



Fig. 9. Distribution of the cluster mass. The dashed and dotted curves represent respectively the total gas mass of the X-ray emitting gas, and the gravitating mass, obtained by assuming hydrostatic equilibrium. Full curves show the uncertainty range for the gravitating mass.

To determine the cluster mass, we use the gas density profile determined from the β model fit (shown in Fig. 6) and gas temperatures in the range of 3.5 to 7 keV. For the temperature profile, we assume a set of models including isothermal models and polytropic models with an index in the range 0.9 to 1.3, and the temperatures fixed to the measured range (3.5 to 7 keV) at the core radius. The resultant uncertainty range for the gravitating mass profiles are shown in Fig. 9, with an isothermal model for $T_{gas} = 5$ keV. The gas mass profile is also shown. At $1 h_{50}^{-1}$ Mpc the total mass of the cluster is in the range $1.6 - 3.7 \cdot 10^{14} M_{\odot}$ (consistent with the results by Burns et al. 1995), and the gas mass fraction is in the range 19 - 44%. If the results are extrapolated to the radius of $3 h_{50}^{-1}$ Mpc, within which a cluster of A2255 is expected to be virialized (e.g., Gunn & Gott, 1972), one finds values of $M_{grav} = 0.45 - 1.3 \cdot 10^{15} M_{\odot}$, and for the gas mass fraction, a range of 33 - 100 %. Typically, the gas mass fraction in clusters is of 10 - 30% (e.g. Böhringer

1995). Therefore, it is likely that in A2255 the true mass of the cluster is closer to the upper limit of the present calculation. This is consistent with the existence in the intracluster plasma of a bulk component with temperature near 7 keV, in addition to the low temperature component detected by ROSAT.

4.3. Radio source confinement



Fig. 10. Allowed range of the pressure of the X-ray emitting gas versus the radial distance from the cluster center (dashed region), for gas temperatures between 3.5 and 7 keV. The equipartition pressures in the tailed radio galaxies (dots) and in the radio halo and relic (dashed lines) are also given.

The gas density and temperature obtained from the X-ray data allow us to derive the thermal pressure of the intergalactic medium. This can be compared with the equipartition pressures within the radio emitting regions, to obtain information about the confinement of the radio sources. The three outermost tailed radio galaxies (1712+638, 1713+643, and 1714+641) are located outside the contours of the X-ray emission and therefore in a region of very low gas density. From the profile of Fig. 6, however, it is evident that all these sources are still in a region where the X-ray brightness is above the background. With the parameters obtained from the fit to the observed brightness profile, a central electron density $n_0 = 1.76 \cdot 10^{-3} \text{ cm}^{-3}$ was obtained. Pressure profiles were derived for temperatures of 3.5 and 7 keV.

In the computation of equipartition parameters for the radio emitting regions, we used standard formulae (Pacholczyk 1970) with the standard assumptions of a low frequency cutoff of 10 MHz, a high frequency cutoff of 100 GHz, equal energy density in protons and electrons, and a filling factor of 1. The values of equipartition magnetic field and minimum internal pressures were computed for the radio halo, for the relic, and for the outermost regions of the tailed radio galaxies.

The comparison between the pressure of the X-ray gas and the equipartition pressures in the radio emitting regions is given in Fig. 10. As already found in other cases (Feretti et al. 1992, 1995, Röttgering et al. 1994), the equipartition pressures of the radio sources are systematically lower by a factor of ~ 10 than the corresponding thermal pressures of the ambient gas. This result implies either that the numerous assumptions used in the calculation of the equipartition pressure are not valid, or that there is a real deviation from the equipartition conditions.

The imbalance between pressures in the diffuse halo and the ambient gas is more dramatic, being a ratio of

about 1000 at the cluster center. To explain this, we cannot simply relax the assumptions made for the computation of equipartition energy, but we may invoke another pressure component, such as thermal gas mixed with the relativistic particles. This is confirmed by the presence of both radio and X-ray emission from the same halo region.

5. Conclusions

Abell 2255 is characterized in the radio domain by several galaxies, and by the presence of diffuse emission consisting of a halo at the cluster center and a more peripheral elongated ridge which we consider a relic. At X-ray wavelengths, the cluster shows an asymmetric structure, suggestive of a merger with the axis in the east-west to southeast-northwest direction.

The existence of a merger is confirmed by the spectral analysis, which enhances a cluster component of temperature $kT = 3.5(\pm 1.5)$ keV, in addition to the higher temperature component of 7.3 keV detected with the Einstein MPC data. A multiphase intracluster medium seems therefore to be associated with this cluster.

The merger process can provide energy to maintain the radio halo. We also stress the need for tailed radio galaxies orbiting at the cluster center to provide the halo relativistic electrons. In the cluster A2255, there are at least three tailed radio galaxies at the cluster center, which are likely to be orbiting at the cluster center. They could be responsible for the continuous supply of relativistic particles to the halo.

The X-ray brightness profile, obtained by averaging azimuthally the count rate in concentric rings around the symmetry center, was fit with the β model, to derive the central density and pressure of the X-ray gas. The internal equipartition pressure in the extended lobes of the cluster radio galaxies is lower by an order of magnitude than the corresponding pressure of the ambient gas. The internal pressure in the halo is lower than the external one by about 3 orders of magnitude.

Acknowledgements. We thank Ger De Bruyn for his help in the radio data calibration, the ROSAT team for providing the processed data, and the EXSAS team for the tools for the data reduction. Thanks are due to Jon Aymon for his careful reading of the manuscript. L.F. acknowledges the MPE of Garching for hospitality and partial financial support.

The WSRT is operated by the Netherlands Foundation for Radio Astronomy with the financial support of ZWO.

References

Böhringer, H., 1995, Seventeenth Texas Symp., Annals of the New York Academy of Sciences, Eds. H. Böhringer, G.E. Morfill, J.E. Trümper, Vol. 759, p. 67
 Briel, U.G., Henry, J.P., Schwarz, R.A., et al., 1991, A&A, 246, L10
 Burns, J.O., Rhee, G., Owen, F.N., Pinkney, J., 1994, ApJ 423, 94

Burns, J.O., Roettiger, K., Pinkney, J., Perley, R.A., Owen, F.N., Voges, W., 1995, ApJ 446, 583
 Cavaliere, A., Fusco-Femiano, R., 1981, A&A, 100, 194
 David, L.P., Sly, A., Jones, C., Forman, W., Vrtilik, S.D., Arnaud, K.A., 1993, ApJ 412, 479
 Edge, A.C., Stewart, G.C., Fabian, A.C., 1992, MNRAS 258, 177
 Evrard, A., Metzler, C., & Navarro, J., 1996, (preprint)
 Fanaroff, B.L., Riley, J.M., 1974, MNRAS 167, 31P
 Fanti, R., 1984, In: Clusters and Groups of Galaxies, Eds. Mardirossian F., Giuricin, G., Mezzetti M., Reidel P.C., Dordrecht, p.185
 Feretti, L., Perola, G.C., Fanti, R., 1992, A&A 265, 9
 Feretti, L., Giovannini, G., 1993, A&A 281, 375
 Feretti, L., Fanti, R., Parma, P., Massaglia, S., Trussoni, E., Brinkmann, W., 1995, A&A 298, 699
 Feretti, L., Giovannini, G., 1996, In: Extragalactic Radio Sources, IAU Symp. 175, Eds. R. Ekers, C. Fanti & L. Padrielli, Kluwer Academic Publisher, in press
 Giovannini, G., Feretti, L., Venturi, T., Kim, K.-T., Kronberg, P.P., 1993, ApJ 406, 399
 Gunn, J.E., Gott, J.R.III, 1972, ApJ 176, 1
 Harris, D.E., Kapahi, V.K., Ekers, R.D., 1980, A&AS 39, 215
 Henry, J.P., Briel, U.G., 1993, Adv. Space Res. 13, (12)191
 Jaffe, W.J., Rudnick, L., 1979, ApJ 233, 453
 Jones, C., Forman, W., 1984, ApJ 276, 38
 O’Dea, C., Owen, F.N., 1986, ApJ 301, 841
 O’Dea, C., Sarazin, C.L., Owen, F. N., 1987, ApJ 316, 113
 Ohashi, T., 1995, Seventeenth Texas Symp., Annals of the New York Academy of Sciences, Eds. H. Böhringer, G.E. Morfill, J.E. Trümper, Vol. 759, p. 217
 Pacholczyk, A.G., 1970, Radio Astrophysics, Freeman and Co., San Francisco.
 Pfeffermann, E., Briel, U.G., Hippmann, H., et al., 1987, Proc. Society for Photo-Optical Instrumentation Engineers (SPIE) 733, 519
 Postman, M., Huchra, J.P., Geller, M.J., 1992, ApJ 384, 404
 Röttgering, H., Snellen, I., Miley, G., et al., 1994, ApJ, 436, 654
 Raymond, J.C., Smith, B.W., 1977, ApJS 35, 419
 Rudnick, L., Owen, F.N., 1977, AJ 82, 1
 Sarazin, C.L., 1986, Rev. Mod. Phys. 58, 1
 Schindler, 1996, A&A, 305, 756
 Struble, M.F., Rood, H.J., 1982, AJ 87, 7
 Trümper, J., 1983, Adv. Space Res. 2, 241
 Zabludoff, A.I., Huchra, J.P., Geller, M.J., 1990, ApJS 74, 1
 Zimmermann, H.U., Becker, W., Belloni, T., Döbereiner, S., Izzo, C., Kahabka, P., Schwentker, O., 1994, EXSAS User’s Guide, MPE Report 244

